JTTEE5 17:708–714
DOI: 10.1007/s11666-008-9276-z
1059-9630/$19.00 © ASM International

Peer Reviewed

Effects of Silver Addition on Properties and Performance of Plasma Sprayed $La_{0.6}Sr_{0.4}Co_{0.2}Fe_{0.8}O_{3-\delta}$ Interconnect Layer

Soodong Park, S. Kumar, Hyuntaek Na, and Changhee Lee

(Submitted April 30, 2008; in revised form September 19, 2008)

Interconnect layers on stainless steel substrates (STS430) for solid oxide fuel cells (SOFC) were built up by atmospheric plasma spraying (APS) using spray dried $La_{0.6}Sr_{0.4}Co_{0.2}Fe_{0.8}O_{3-\delta}$ (LSCF) and blended LSCF/Ag composites. The microstructure and phase of each coating were analyzed using scanning electron microscopy (SEM) and x-ray diffraction (XRD) studies, respectively. Furthermore, bond strength, microhardness, performance in a thermal cycle test and in an oxidation test, and electrical conductivity were measured and compared. The coatings prepared from spray dried LSCF have higher porosity and more cracks within the splats and at intersplat boundaries. In contrast, the coatings prepared from LSCF/Ag had fewer cracks and less porosity due to the relatively high ductility of silver. After oxidation testing at 800 °C for 200 h, the weight change of the STS430 substrate and the LSCF and LSCF/Ag-coated alloys were found to be 0.06833, 0.01950, and 0.01656 mg/cm^2, respectively. Also the electrical conductivity of LSCF and LSCF/Ag coatings were higher than that of STS430 by two orders.

Keywords Ag, atmospheric plasma spraying, interconnect, $La_{0.6}Sr_{0.4}Co_{0.2}Fe_{0.8}O_{3-\delta}$, solid oxide fuel cell (SOFC)

1. Introduction

A solid oxide fuel cell (SOFC) is a device that directly converts chemical energy into electrical energy (Ref 1, 2). Among all components in a SOFC, the interconnect plays an important role. The primary function of the SOFC interconnect is to connect the anode of one cell to the cathode of the adjacent cell for an electrical series arrangement, thereby preventing the mixing of fuel and the oxidant gases. In general, the interconnect has to meet the following demands:

- High electronic and low ionic conductivities (electrical conductivity > 1 Scm^{-1})
- Chemical stability under the reducing and oxidizing conditions at the anode and cathode sides, respectively, of the cell at temperatures up to 1000 °C (range of oxygen activity 10^{-18} to 10^{-8} atm)
- Gas tightness
- Thermal expansion coefficient matching with that of other cell components
- Easy manufacture and low cost

In recent years, ferritic stainless steels have been developed as alternative to ceramic interconnects. However, ferritic stainless steel interconnects have some limitations such as the formation of insulating oxide scales during high-temperature operation. Chromium-based oxides tend to form on the surface of interconnects. The electrical conductivity of chromia at 800 to 1000 °C has been reported to be 1 to 5 $\times$ 10^{-2} Scm^{-1} (Ref 3, 4). Also, the vaporization of volatile chromium species from the metallic interconnect can lead to severe degradation of the electrical properties of SOFC. A description of the degradation mechanism was reported by Hilpert et al. (Ref 5). It is based on the vaporization of Cr_2O_3 on the interconnect surface as $CrO_3(g)$ or $CrO_2(OH)_2(g)$ as major gaseous species with chromium in the 6^+ oxidation state. The vapor species are reduced at the three-phase boundary by electrochemical reaction forming $Cr_2O_3(s)$. The Cr_2O_3 or the reaction products formed inhibit the oxygen reduction necessary for the operation of the SOFC and lead to polarization losses (Ref 5, 6). Hence, ferritic stainless steel has to be protected by a coating layer suited for high-temperature SOFC operation, which can be produced for instance using APS (Ref 7).

This article is an invited paper selected from presentations at the 2008 International Thermal Spray Conference and has been expanded from the original presentation. It is simultaneously published in *Thermal Spray Crossing Borders, Proceedings of the 2008 International Thermal Spray Conference*, Maastricht, The Netherlands, June 2-4, 2008, Basil R. Marple, Margaret M. Hyland, Yuk-Chiu Lau, Chang-Jiu Li, Rogerio S. Lima, and Ghislain Montavon, Ed., ASM International, Materials Park, OH, 2008.

Soodong Park, S. Kumar, Hyuntaek Na, and **Changhee Lee**, Division of Advanced Materials Science & Engineering, Hanyang University, 17 Haengdang-dong, Seongdong-ku, Seoul 133-791, South Korea. Contact e-mails: chlee@hanyang.ac.kr, airtwenty4@hanyang.ac.kr, hai_kumars@rediffmail.com and nht6480@hanyang.ac.kr

Many different coating technologies have been applied to fabricate coating layers on metallic interconnects, including electrochemical vapor deposition (EVD), chemical vapor deposition (CVD), physical vapor deposition (PVD), tape casting, screen printing, sol-gel, and thermal spraying methods (Ref 8-13). Thermal spraying techniques, especially atmospheric plasma spraying (APS), seem to be economically attractive and effective techniques for industrial production of SOFCs due to its low cost, easy operation, high deposition efficiency, ability to coat large surfaces, wide selection of materials, and so forth. In this study, coating layers for SOFC interconnects were deposited using APS.

A high density of pores and cracks were obtained in the thermally sprayed ceramic coating layers produced in a previous study. Therefore, the cracks were interconnected through vertical microcracks in the individual splats within the coating, allowing gas or liquids to propagate throughout the coating. This leads to the generation of oxide scales on metallic interconnects during long-term operation of the SOFC. In this study, silver powder was added to the ceramic feedstock as a crack-reducing means.

Table 1 The APS process parameters

Plasma gas composition		Arc current, A	Distance, mm	Powder feed rate, g/min
Ar, SCFH (a)	H_2, SCFH			
100	5/10/15	500	100	10

(a) SCFH, standard cubic feet per hour (1 SCFH = 0.47 lpm)

2. Experiments

2.1 Atmospheric Plasma Spraying

Two kinds of coatings were deposited by an atmospheric plasma spray system (Sulzer Metco 9 MB, Switzerland) from different feedstock materials. A mixture of argon and hydrogen served as plasma process gas for these experiments, where argon was also used as powder carrier gas. The spraying distance between the substrate and the exit of the nozzle was maintained at 100 mm. The feedstock powder was vertically injected into the plasma jet center downstream of the exit with a feed rate of 10 g/min. In order to change the characteristics of the plasma jet, the hydrogen gas flow rate was changed while the other process parameters were kept constant. The processing parameters are tabulated in Table 1. The feedstock powders were spray deposited on grit-blasted STS430 stainless steel plates.

2.2 Feedstock Characterization

Prior to spraying, characterization of the blended powder feedstock was performed. Feedstock powders used for this study were spray dried $La_{0.6}Sr_{0.4}Co_{0.2}Fe_{0.8}O_{3-\delta}$ (LSCF) and blended LSCF/Ag. LSCF/Ag composite powder with 25 wt.% of Ag were produced via mechanical mixing using the mixer TURBULA (WAB, Willy A, Bachofen AG Maschinenfabrik, Basel, Switzerland) with a rotational speed of 30 rpm. The mixing time was 5 h. The characterization of the powder feedstocks were performed using scanning electron microscopy (SEM). Figure 1 shows SEM

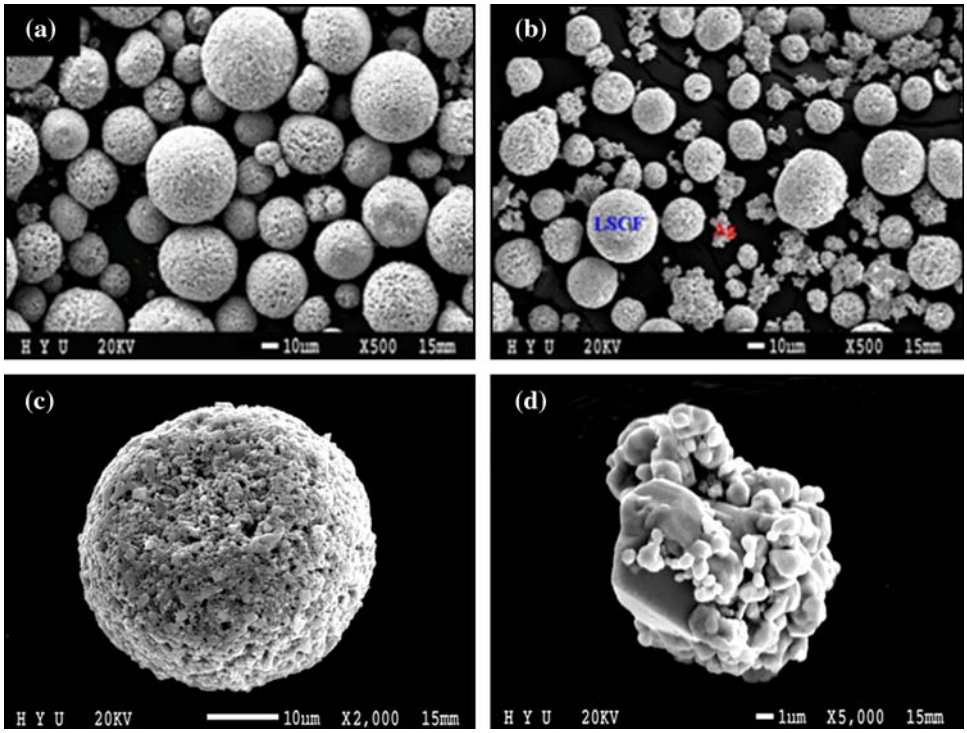

Fig. 1 Scanning electron images of feedstock materials. (a) $La_{0.6}Sr_{0.4}Co_{0.2}Fe_{0.8}O_{3-\delta}$. (b) LSCF/Ag. (c) Individual LSCF powder particle. (d) Individual silver powder particle

images of each feedstock powder. Figure 1(a) shows the SEM image of the spray dried LSCF powder. Figure 1(b) displays the SEM image of LSCF blended with Ag powder. Figures 1(c) and (d) are individual LSCF and silver powder particles, respectively. The morphology of LSCF and silver particles are nearly spherical and dendritic, respectively. The average particle sizes of LSCF and Ag powders are 30 to 40 μm and 10 to 40 μm, respectively. The characteristics of the feedstock are tabulated in Table 2.

2.3 Characterization of Coating

The microstructure of the coatings was observed through scanning electron microscopy (SEM) with a JEOL microscope, and the phase compositions of each condition were measured using a D/MAX-2500/PC x-ray diffractometer (XRD). The porosity of the coatings was measured using an image analysis method, and the area fraction of the porosity was calculated by Image Pro-Plus software. Cross sections of coatings were polished as smooth as a mirror. Up to 20 SEM images (magnification: 300×) of the cross sections of each sample were taken for the analysis. The software Image-Pro Plus can be used to estimate the percentage of open pores in a selected area. The software used for image analysis procedure is Image-Pro Plus 6.0 (Media Cybernetics, USA).

Table 2 Characteristics of the feedstock

Powder	Size, μm	Morphology	Density, g/cm^3	Melting point, °C
LSCF	−40 + 30	Spherical	2.30	···
Silver	−40 + 10	Irregular	10.49	961.93

Vickers microhardness was measured on polished surfaces using an applied load of 1.961 N. Bond strength was measured using Romulus Bond Strength tester. For the thermal cycle test, the samples were put in a furnace at 800 °C for 1 h and then quenched in water. Twenty continuous cycles were performed on each sample. Oxidation tests were performed in the same way. The samples were heat treated at 800 °C for 20 h and allowed to quench in air. After measuring the weight gain, the samples were put again in the furnace and the same process was done for 200 h with 20 h intervals. Samples of STS430 substrate coatings prepared from LSCF and LSCF/Ag blend were oxidized at 800 °C for 200 h for measuring the electrical conductivity using direct current (DC) quasi-four-probe method. Keithley 2430 Source Meter and 2000 Digital Multi-Meter were used for this measurement, and the samples were tested for 80 h at 800 °C. Samples used for this study were 5 × 5 × 1 mm. After oxidation at 800 °C for 200 h, the electrical conductivity of coated STS430 samples was measured.

3. Results and Discussion

3.1 Microstructure

Figure 2 shows the SEM images of the as-sprayed coatings prepared from LSCF (a) to (c) and LSCF/Ag powder (d) to (f) with different hydrogen gas flow rates. In the case of LSCF coatings, the porosity decreases and crack content is reduced with increasing hydrogen gas flow rate. However, the cracks could not be controlled for all

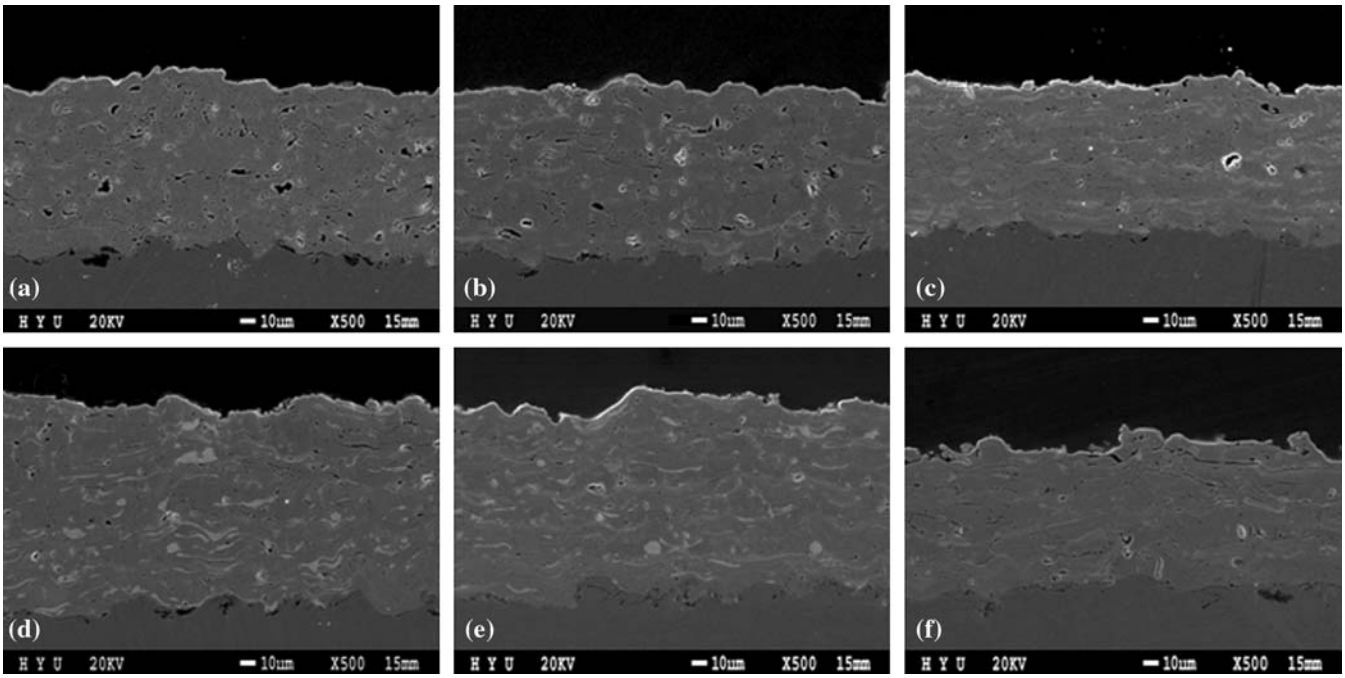

Fig. 2 Cross-sectional SEM images of LSCF and LSCF/Ag coatings at different hydrogen flow rates (SCFH). (a) $5H_2$ LSCF. (b) $10H_2$ LSCF. (c) $15H_2$ LSCF. (d) $5H_2$ LSCF/Ag. (e) $10H_2$ LSCF/Ag. (f) $15H_2$ LSCF/Ag

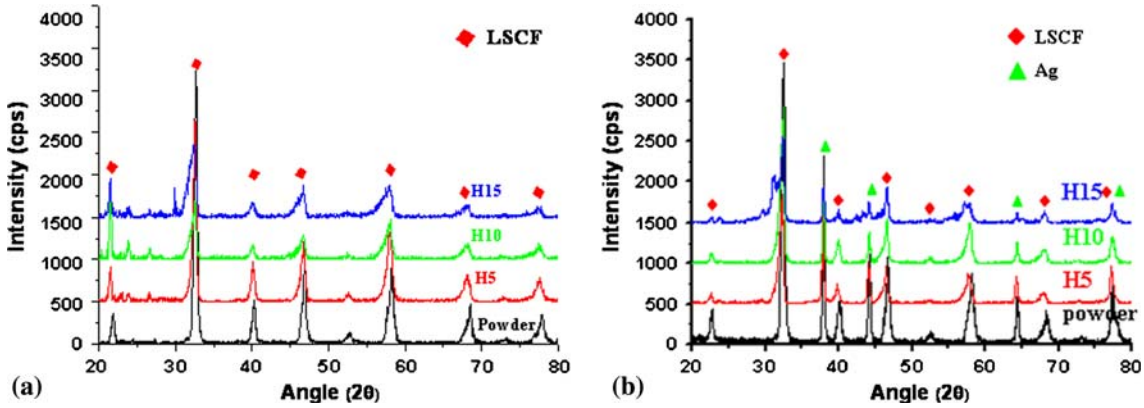

Fig. 3 X-ray diffraction patterns of feedstock and coatings, sprayed with different hydrogen content in the plasma. (a) LSCF and (b) LSCF/Ag

process parameters. Hence, silver was added to the LSCF as crack reducing agent. When silver is added, porosity increases with increasing hydrogen gas flow rate. Especially at a hydrogen flow rate of 15 SCFH, the silver content in the coating was reduced abruptly as consequence of increased silver evaporation. At 5 and 10 SCFH hydrogen gas flow rates, the quantity of silver remaining in the coating was 4.81 and 3.98%, respectively. In case of 15 SCFH, the Ag content was reduced to 1.06% because of the higher enthalpy of the plasma jet.

Figures 3(a) and (b) show the XRD patterns of plasma sprayed LSCF and LSCF/Ag coatings at different processing conditions. X-ray diffraction patterns indicate that peaks are almost similar for all conditions with two exceptions: with the high hydrogen content in the plasma (15 SCFH) the LSCF starts to decompose as seen by the new small peak left of the main peak at about 30°, and in the case of LSCF with Ag the peak intensity for silver is reduced because of high plasma enthalpy resulting in evaporation.

3.2 Mechanical Properties

Figure 4 shows the microhardness results for the coatings prepared from different feedstock powders with different plasma parameters. From Fig. 4 it becomes clear that increasing hydrogen gas flow rate increases the microhardness values for both feedstocks. The microhardness values for coatings prepared from LSCF powder at 5, 10, and 15 SCFH hydrogen flow rates are 380, 404, and 412 HV, respectively. The values for LSCF with silver are 255, 289, and 356 HV, respectively. It is also clear that adding silver with LSCF reduces the microhardness values for all plasma parameters. However, the difference is diminished at higher hydrogen gas flow rates again as a result of increased silver evaporation.

Figure 5 shows the porosity values for the coatings prepared with both powders. For coatings prepared from LSCF powder at 5, 10, and 15 SCFH, the porosity values are 2.08, 2.038, and 1.347%, respectively. The values for coatings prepared from LSCF with silver are 0.713, 0.813, and 1.542%, respectively. It is clear from the data that

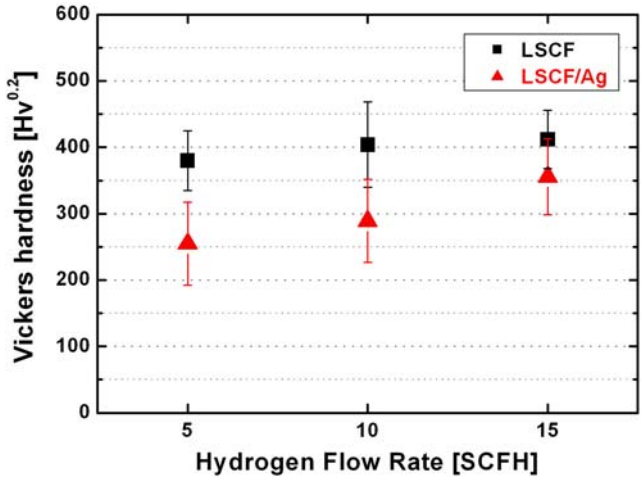

Fig. 4 Vickers microhardness values for coatings as a function of hydrogen gas flow rate prepared from LSCF and LSCF/Ag powders

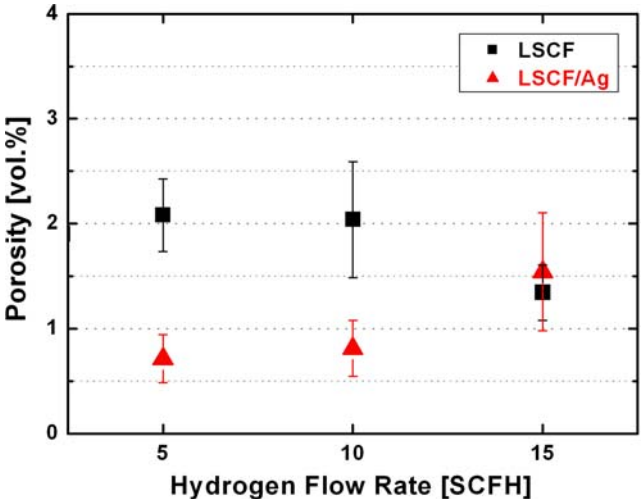

Fig. 5 Porosity of coatings as a function of hydrogen gas flow rate prepared from LSCF and LSCF/Ag powder

with increasing hydrogen flow rate the porosity decreases in the case of LSCF powder. The result is opposite for LSCF with silver. This effect is clearly due to the silver evaporation. However, the porosity value of the coating is lower for the powder with silver addition. Figure 6 shows the bond strength data of the coatings. The bond strength values for the coatings prepared from LSCF with silver were higher for all the applied plasma parameters.

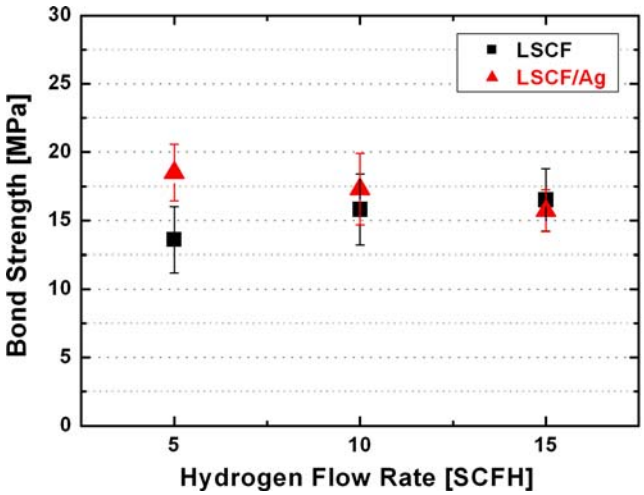

Fig. 6 Bond strength values of coatings as a function of hydrogen gas flow rate prepared from LSCF and LSCF/Ag powders

3.3 Thermal Cycle Test

Figures 7(a) and (c) show the SEM images of the coatings prepared at 5 SCFH of hydrogen from LSCF and LSCF with silver after thermal cycle testing. It is obvious that after testing coatings prepared from LSCF powder have many pores and cracks. The cracks are interconnected with each other, which leads to propagation effects. Coatings prepared from LSCF with silver show lower porosity and very few cracks. Figures 7(b) and (d) show the magnified images of the respective coatings. The silver layer can be seen in the coating where it acts as a crack-reducing agent.

3.4 Oxidation Test

Figure 8 shows the results of the oxidation test. In the figure, the weight gain caused by oxidation is illustrated for STS430 (the substrate), and for such substrates with a coating prepared from LSCF powder and from LSCF with silver, as well. It can be seen from the figure that the weight gain abruptly increased for the substrate material within 20 h. There was no such dramatic increase observable in the case of substrates with coatings prepared from LSCF and LSCF with silver. After 20 h, the weight gain was gradual for all the three samples. The change in weight for STS430 and substrates with coatings prepared from LSCF and LSCF with silver were 0.06833, 0.0195, and 0.01656 mg/cm^2, respectively. Hence, it is clear that addition of silver to the LSCF powder increases the resistance against oxidation of the coatings. Figures 9(a),

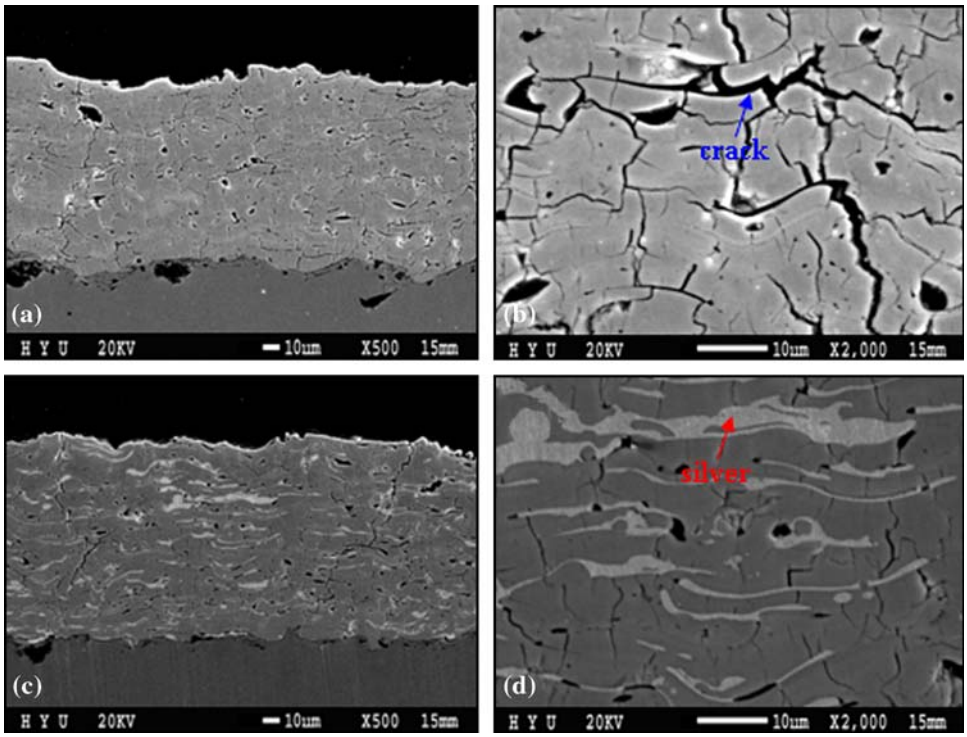

Fig. 7 Scanning electron images of the cross-sectional microstructure after 20 thermal cycle tests. (a) LSCF (5H_2 SCFH flow rate). (b) Magnified image. (c) LSCF/Ag (5H_2 SCFH flow rate). (d) Magnified image

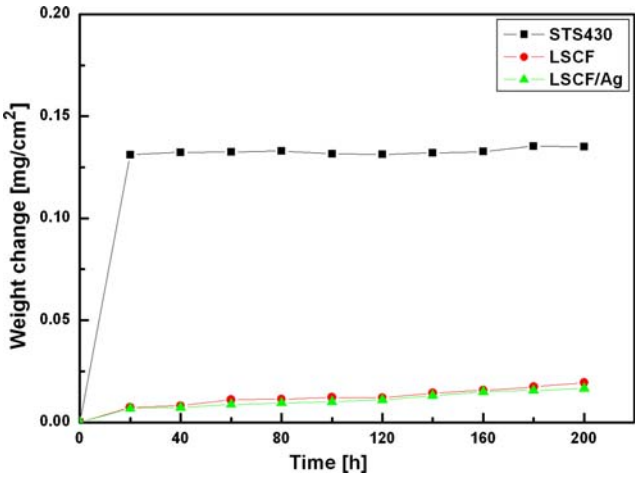

Fig. 8 Weight change with time during oxidation of STS430 alloy, alloy coated with LSCF and LSCF/Ag at 800 °C in air

(b), and (c) show the top view of the oxidized samples of STS430 and coatings prepared from LSCF and LSCF/Ag, respectively. Figures 9(d) to (f) show the x-ray diffraction results of oxidized and as-sprayed coatings. The uncoated substrate oxidized severely and formed chromium, iron, and manganese based oxides. However, coatings prepared from LSCF and LSCF/Ag show no significant phase changes after oxidation test.

3.5 Electrical Conductivity

Figure 10 shows the high-temperature transversal electrical conductivity of STS430 substrate and coatings prepared from LSCF and LSCF/Ag after oxidation at 800 °C for 200 h. It can be seen from the figure that for coatings, the conductivity values are much higher than for the STS430 substrate alone. Up to a certain time period, increasing time does not affect the conductivity value of the substrate. At the earlier state of the process, the oxides

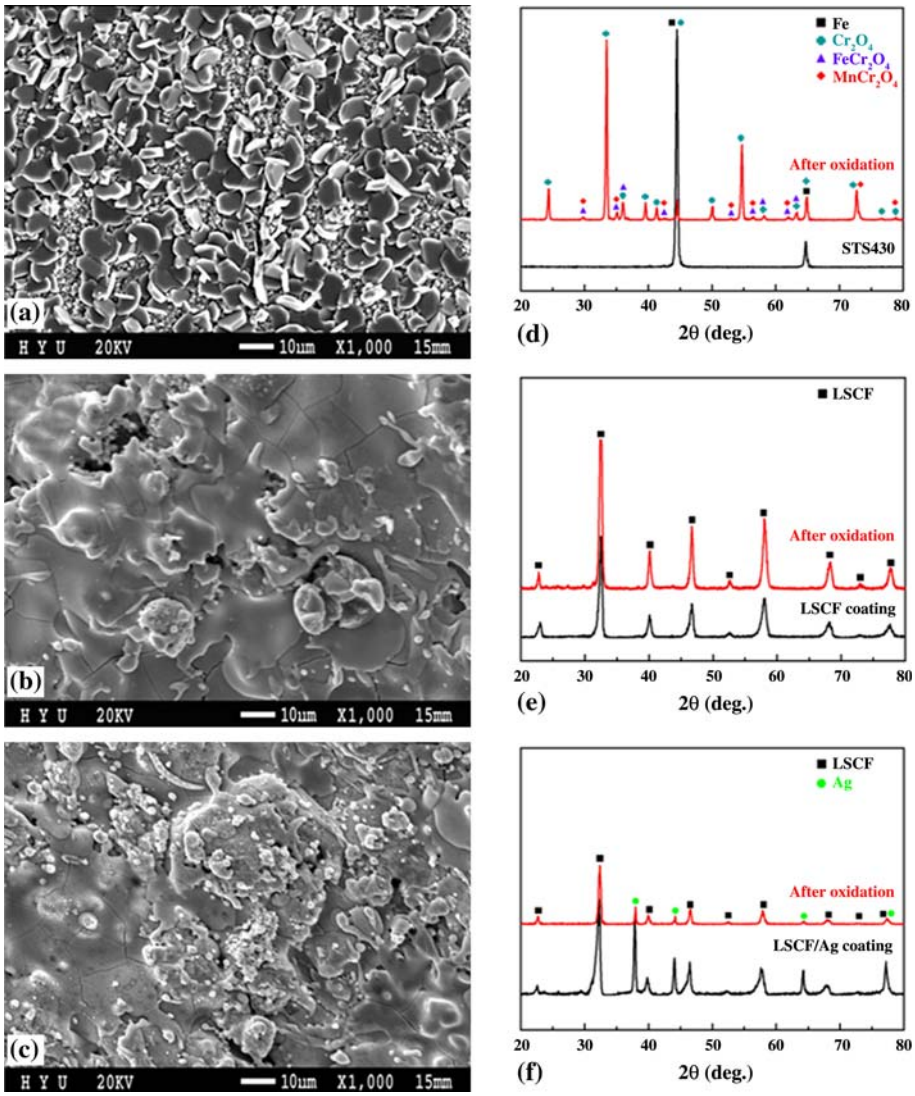

Fig. 9 Scanning electron microscopy images and x-ray patterns of STS430 alloy. (a) and (b), LSCF coated (c) and (d) and LSCF/Ag coated alloy (e) and (f), respectively, after the oxidation test

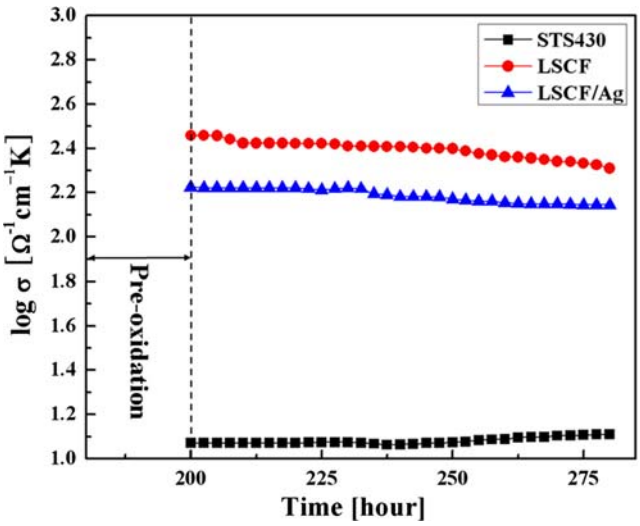

Fig. 10 Transversal electrical conductivity of STS430, and STS430 coated with LSCF and LSCF/Ag, respectively, measured at 800 °C in air

present in the substrate consist of Cr_2O_3, mostly. With increasing time, the formation of $(Mn,Cr)_3O_4$, which has a spinel structure, takes place. Hence the conductivity increases slightly. Coatings prepared from LSCF have a relatively higher conductivity than that of LSCF/Ag. LSCF has a perovskite structure in which the electrical conductivity is lattice defect dominated. Hence, the addition of silver to the LSCF decreases the electrical conductivity. The electrical conductivity after 200 h annealing time of the STS430 substrate was 1.08737 log [Ω^{-1} cm^{-1} K] and the same for STS430/LSCF and for STS430/LSCF/Ag were 2.36211 log [Ω^{-1} cm^{-1} K] and 2.15488 log [Ω^{-1} cm^{-1} K], respectively. The reduction of the electrical conductivity for LSCF and LSCF/Ag coatings between 200 and 280 h interval were 0.05203 log [Ω^{-1} cm^{-1} K] and 0.01016 log [Ω^{-1} cm^{-1} K], respectively. Hence for long-term application, LSCF in addition to silver seems to be advantageous.

4. Conclusions

Interconnect layers were built up by coating ferritic stainless steel substrates (STS430) by atmospheric plasma spraying (APS) using spray dried LSCF and blended LSCF/Ag powders. The coatings with silver addition were denser with fewer cracks and lower porosity than that of powders without silver. After oxidation testing for 200 h, the change in weight for substrates coated with LSCF and LSCF with silver were 0.0195 and 0.01656 mg/cm^2, respectively. The compactness and oxidation resistance at 800 °C of LSCF coatings can be significantly promoted by adding the ductile Ag. This is due to the effective barrier to inward oxygen migration by the tamping effect of Ag at the interparticle boundaries within the coating.

Acknowledgment

This work was financially supported by the Korea Science and Engineering Foundation (KOSEF) through the National Research Laboratory (NRL) program (No. 2006-02289).

References

1. N.Q. Minh and T. Takahashi, Selected Reference Relevant to Solid Oxide Fuel Cell Technology, *Sci. Technol. Ceram. Fuel Cells,* 1995, p 351-353
2. N.Q. Minh, A. Anumakakonda, B. Chung, R. Doshi, J. Ferrall, G. Lear, K. Montgomery, E. Ong, L. Schipper, and J. Yamanis, High-Performance, Reduced-Temperature SOFC Technology, *Fuel Cells Bull.*, 1999, **2**, p 9-11
3. A. Holt and P. Kofstadt, Electrical Conductivity and Defect Structure of Mg-Doped Cr_2O_3, *Solid State Ionics*, 1997, **100**, p 201-209
4. A. Holt and P. Kofstadt, Electrical Conductivity of Cr_2O_3 Doped with TiO_2, *Solid State Ionics*, 1999, **117**, p 21-25
5. D. Das, M. Miller, H. Nickel, and K. Hilpert, Chromium Evaporation from SOFC Interconnector Alloys and Degradation Process by Chromium Transport, *Europ. SOFC Forum*, 1994, **2**, p 703
6. K. Hilpert, D. Das, M. Miller, D.H. Peck, and R. Weiß, Chromium Vapour Species over SOFC Interconnect Materials and their Potential for Degradation Processes, *J. Electrochem. Soc.*, 1996, **143**, p 3642
7. R. Zheng, X.M. Zhou, S.R. Wang, T.L. Wen, and C.X. Ding, A Study of Ni + 8YSZ/8YSZ/$La_{0.6}Sr_{0.4}CoO_{3-\delta}$ ITSOFC Fabricated by Atmospheric Plasma Spraying, *J. Power Sources*, 2005, **140**, p 217-225
8. A.O. Isenberg, Energy Conversion via Solid Oxide Electrolyte Electrochemical Cells at High Temperatures, *Solid State Ionics*, 1981, **3-4**, p 431-437
9. J. Will, A. Mitterdorfer, C. Kleinlogel, D. Perednis, and L.J. Gauckler, Fabrication of Thin Electrolytes for Second-Generation Solid Oxide Fuel Cells, *Solid State Ionics*, 2000, **131**, p 79-96
10. D. Simwonis, H. Thulen, F.J. Dias, A. Naoumidis, and D. Stöver, Properties of Ni/YSZ Porous Cermets for SOFC Anode Substrates Prepared by Tape Casting and Coat-Mix Process, *J Mater. Process Technol.*, 1999, **92-93**, p 107
11. J. Van Herle, R. lhringer, R. Vasquez Cavieres, L. Constantin, and O. Bucheli, Anode Supported Solid Oxide Fuel Cells with Screen-Printed Cathodes, *J. Europ. Ceram. Soc.*, 2001, **21**, p 1855-1859
12. W. Qu, J. Li, and D.G. Ivey, Sol-Gel Coatings to Reduce Oxide Growth in Interconnects Used for Solid Oxide Fuel Cells, *J. Power Sources*, 2004, **138**, p 162-173
13. O. Kwon, S. Kumar, S. Park, and C. Lee, Comparison of Solid Oxide Fuel Cell Anode Coatings Prepared from Different Feedstock Powders by Atmospheric Plasma Spray Method, *J. Power Sources*, 2007, **171**, p 441-447